

Quench dynamics of the Schwinger model via variational quantum algorithms

Lento Nagano^{✉*}

*International Center for Elementary Particle Physics (ICEPP), The University of Tokyo,
7-3-1 Hongo, Bunkyo-ku, Tokyo 113-0033, Japan*

Aniruddha Bapat and Christian W. Bauer[†]

Lawrence Berkeley National Laboratory, 1 Cyclotron Road, Berkeley, California 94720, USA

 (Received 7 April 2023; revised 20 June 2023; accepted 5 July 2023; published 2 August 2023)

We investigate the real-time dynamics of the $(1 + 1)$ -dimensional $U(1)$ gauge theory known as the Schwinger model via variational quantum algorithms. Specifically, we simulate quench dynamics in the presence of an external electric field. First, we use a variational quantum eigensolver to obtain the ground state of the system in the absence of an external field. With this as the initial state, we perform real-time evolution under an external field via a fixed-depth, parameterized circuit whose parameters are updated using McLachlan's variational principle. We use the same ansatz for initial-state preparation and time evolution, by which we are able to reduce the overall circuit depth. We test our method with a classical simulator and confirm that the results agree well with exact diagonalization.

DOI: [10.1103/PhysRevD.108.034501](https://doi.org/10.1103/PhysRevD.108.034501)

I. INTRODUCTION

Lattice gauge theory is a powerful tool for studying quantum field theory. In the conventional approach, simulations are performed using the Monte Carlo method, which requires the exponential of the Euclidean action $\exp(-S_E)$ to be positive and real. This protocol suffers from a sign problem when we consider e.g. a topological term, a finite chemical potential, and real-time dynamics.

Instead of Monte Carlo, one can use the Hamiltonian formalism, which avoids the sign problem as it is not a sampling-based approach. However, the quantum state grows exponentially with the size of the system, making this approach not feasible on classical computers. The advantage of quantum computers is that the computational resources can be kept logarithmic in system size, as was shown in the seminal paper by Jordan, Lee, and Preskill [1]. Since that work, digital quantum simulation in the context of quantum field theory has been attracting a lot of interest [2–65]. In particular, real-time simulation is one of the important applications since it can in general not be captured efficiently by any known classical method.

The standard simulation method on quantum computers uses Suzuki-Trotter decomposition, where the circuit depth increases as the evolution time does, which causes a decoherence problem on noisy intermediate-scale quantum (NISQ) devices. Variational algorithms combine quantum computations with classical optimizations, and are able to perform both state preparation and time evolution using an approach called variational quantum simulation (VQS), even if the accuracy of the method depends on the chosen variational ansatz. A VQS method based on McLachlan's variational principle (MVP) was proposed in [66,67] in which the evolved states are approximated by parametrized states (ansatz) with a fixed depth.¹

In this work, we apply this variational method to investigate the real-time dynamics of $(1 + 1)$ -dimensional $U(1)$ gauge theory called the Schwinger model.² Specifically, we perform real-time simulation after turning on an external electric field to see electron-positron pair creations induced by the external field, which is the so-called Schwinger mechanism [87]. This is similar to what was considered in [88] where a classical tensor network approach was used.³

*lento@icepp.s.u-tokyo.ac.jp

†cwbauer@lbl.gov

Published by the American Physical Society under the terms of the Creative Commons Attribution 4.0 International license. Further distribution of this work must maintain attribution to the author(s) and the published article's title, journal citation, and DOI. Funded by SCOAP³.

¹See [68–84] for algorithmic developments of the original algorithm and other variational methods for real-time simulation. See also [85] for a recent review.

²The authors [86] proposed an application of the variational method to a scalar field theory and performed adiabatic-state preparation, while they did not provide an explicit real-time simulation.

³See also [89] for a recent study in a slightly different setup by using VQE and Suzuki-Trotter decomposition.

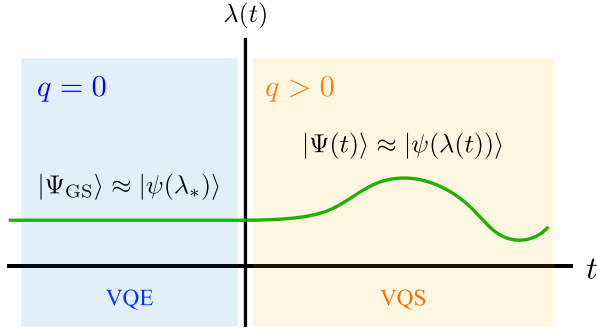


FIG. 1. Sketch of our simulation. We start from the ground state in the absence of external electric field q . We then suddenly turn on the external field q and evolve the state via the Hamiltonian with $q > 0$. These states are approximated by the same ansatz $|\psi(\lambda)\rangle$.

See Fig. 1 for the sketch of our simulation protocol. We first prepare the ground state $|\Psi_{\text{GS}}\rangle$ in the absence of the external electric field q by using a variational quantum eigensolver (VQE). At initial time $t=0$ the external field is then suddenly turned on (the quantum quench), and the time evolution in the system with an external electric field is then studied. We approximate the dynamical states $|\Psi(t)\rangle = e^{-iH_{q \neq 0}t}|\Psi_{\text{GS}}\rangle$ by the same ansatz used in VQE, and evolve the parameters according to MVP. Note that by performing both state preparation and time evolution through variational circuits, the depth of a quantum circuit is greatly reduced.

The structure of this paper is organized as follows. Section II introduces the Hamiltonian of the Schwinger model and observables we will focus on. Section III explains a method we will use for the simulation. In Sec. IV results are presented and compared them with exact diagonalization. Finally, conclusions are given in Sec. V.

II. THE SCHWINGER MODEL

The Schwinger model describes quantum electromagnetism in one spatial and one time dimension. This model is relatively simple, and can in fact be solved analytically [90,91] in the massless limit. It is nevertheless a very interesting field theory to study, since despite its simplicity it shares several features with the QCD, the theory of the strong interaction, such as confinement and charge screening [92,93].

A. Lattice Hamiltonian and spin description

Here we will define the lattice Hamiltonian and introduce its spin description. We mostly follow the convention used in [10]. First of all, the Lagrangian of the continuum Schwinger model is given by

$$\mathcal{L}_{\text{con}} = -\frac{1}{4}F_{\mu\nu}F^{\mu\nu} + i\bar{\psi}\gamma^\mu(\partial_\mu + igA_\mu - m)\psi + \frac{g\theta}{4\pi}\epsilon_{\mu\nu}F^{\mu\nu}. \quad (1)$$

Here the first two terms correspond to the kinetic term of the gauge boson and fermion, respectively, while the third term denotes a topological term that does not affect the classical equations of motion, but does affect the quantum spectrum.

Taking the gauge $A_0 = 0$ and introducing the canonical momentum $\Pi := \partial\mathcal{L}_{\text{con}}/\partial(\partial_0 A^1)$, we can write the continuum Hamiltonian as

$$\int dx \left[\frac{1}{2} \left(\Pi - \frac{g\theta}{2\pi} \right)^2 - i\bar{\psi}\gamma^1(\partial_1 + igA_1 - m)\psi \right],$$

with $\Pi = \partial_0 A^1 + g\theta/2\pi$. As is usual in $A_0 = 0$ gauge, Gauss's law has to be enforced through an extra constraint, and physical states have to satisfy $G|\text{phys}\rangle = 0$ with $G = \partial_1 \Pi + g\psi^\dagger\psi$.

A lattice version of this Hamiltonian can be obtained following the work of [94]. Fermions are put on a staggered lattice, where the position x is sampled at discrete points x_n . Here $n = 0, \dots, N-1$ label the lattice sites corresponding to $x_n = na$, and a is the lattice spacing. The fermion fields at each lattice site are written in terms of χ_n , which represents the Dirac fermion $\psi(x) = (\psi_u(x), \psi_d(x))^T$ through

$$\frac{\chi_n}{\sqrt{a}} \leftrightarrow \begin{cases} \psi_u(x_n) & (n: \text{even}) \\ \psi_d(x_n) & (n: \text{odd}) \end{cases}. \quad (2)$$

The gauge fields are represented through operators living on the links between n th and $(n+1)$ th lattice sites

$$U_n \leftrightarrow e^{-iagA^1(x_n)}, \quad (3)$$

$$L_n \leftrightarrow -\Pi(x_n)/g. \quad (4)$$

These lattice variables satisfy the commutation relations

$$\begin{aligned} \{\chi_n^\dagger, \chi_m\} &= \delta_{mn}, \\ \{\chi_n, \chi_m\} &= 0, \\ [U_n, L_m] &= \delta_{mn}U_n, \end{aligned}$$

and $U_n^\dagger = U_n^{-1}$, $L_n^\dagger = L_n$. With these definitions, the lattice Hamiltonian is given by

$$\begin{aligned} H = J \sum_{n=0}^{N-2} (L_n + q)^2 - iw \sum_{n=0}^{N-2} (\chi_n^\dagger U_n \chi_{n+1} - \chi_{n+1}^\dagger U_n^\dagger \chi_n) \\ + m \sum_{n=0}^{N-1} (-1)^n \chi_n^\dagger \chi_n, \end{aligned} \quad (5)$$

where $w = 1/(2a)$, $J = g^2 a/2$ and $q = \theta/(2\pi)$. Introducing nonzero q corresponds to turning on the external electric field.

Gauss's law gives a constraint for the L_n links on the lattice given by

$$L_n - L_{n-1} = \chi_n^\dagger \chi_n - \frac{1 - (-1)^n}{2}. \quad (6)$$

We impose the open boundary condition $L_{-1} = 0$ and fix the gauge $U_n = 1$ to eliminate gauge fields from the Hamiltonian.

One can transform the above Hamiltonian into a spin Hamiltonian through the Jordan-Wigner transformation [95],

$$\chi_n = \frac{X_n - iY_n}{2} \prod_{i=0}^{n-1} (-iZ_i). \quad (7)$$

This leads to the spin Hamiltonian given by

$$H = J \sum_{n=0}^{N-2} \left[\sum_{i=0}^n \frac{Z_i + (-1)^i}{2} + q \right]^2 + \frac{w}{2} \sum_{n=0}^{N-2} [X_n X_{n+1} + Y_n Y_{n+1}] + \frac{m}{2} \sum_{n=0}^{N-1} (-1)^n Z_n, \quad (8)$$

up to an irrelevant constant.

B. Observables

While there are several observables one can study in the Schwinger model, in this work we focus on three observables [88,96]. The first one is the total electric field,

$$\mathcal{E}(t) = \frac{g}{N} \sum_{n=0}^{N-1} \langle L_n + q \rangle_t, \quad (9)$$

where $\langle \bullet \rangle_t := \langle \psi(t) | \bullet | \psi(t) \rangle$. In the spin description this is given by

$$\mathcal{E}(t) = \frac{g}{2N} \sum_{n=0}^{N-1} \sum_{k=0}^n \langle Z_k \rangle_t + \frac{g}{2N} \sum_{n=0}^{N-1} \sum_{k=0}^n (-1)^k + gq. \quad (10)$$

The second observable is the chiral condensate $\langle \bar{\psi} \psi \rangle$ whose lattice counterpart is given by

$$\Sigma(t) = \frac{ag}{N} \sum_{n=0}^{N-1} (-1)^n \langle \chi_n^\dagger \chi_n \rangle_t \quad (11)$$

$$= \frac{ag}{N} \sum_{n=0}^{N-1} (-1)^n \langle Z_n \rangle_t, \quad (12)$$

up to an irrelevant constant. In the heavy mass regime $m \gg g$ this can be interpreted as the expectation value of the particle number operator, while this interpretation is not

exact in other regimes. Nonetheless, this gives an approximate metric for particle-antiparticle creation.

The third and final observable is the U(1) charge Q defined by

$$Q = \frac{1}{N} \sum_{n=0}^{N-1} \langle Z_n \rangle_t. \quad (13)$$

This observable is useful since it has to be preserved in the evolution under the Hamiltonian (8).

III. METHOD

A. Ansatz

As already discussed, this study uses variational quantum circuits for both the state preparation and the time evolution of the system after the quantum quench. To create the initial ground state in the theory without an external electric field we use the Hamiltonian variational ansatz (HVA) [97–99] defined as

$$|\psi(\boldsymbol{\alpha}, \boldsymbol{\beta}, \boldsymbol{\gamma})\rangle = U_{L-1} \cdots U_0 V_{\text{init}} |0\rangle, \quad (14)$$

where

$$V_{\text{init}} = \prod_{n:\text{even}} X_n, \quad (15)$$

$$U_l(\boldsymbol{\alpha}_l, \boldsymbol{\beta}_l, \boldsymbol{\gamma}_l) = \prod_{n=0}^{N-1} u_n^{(Z)}(\gamma_{l,n}) \times \prod_{n:\text{odd}} u_n^{(ZZ)}(\beta_{l,n}) \prod_{n:\text{even}} u_n^{(ZZ)}(\beta_{l,n}) \times \prod_{n:\text{odd}} u_n^{(XY)}(\alpha_{l,n}) \prod_{n:\text{even}} u_n^{(XY)}(\alpha_{l,n}), \quad (16)$$

with

$$u_n^{(Z)}(\gamma_{l,n}) = \exp \left[i \frac{\gamma_{l,n}}{2} Z_n \right], \quad (17)$$

$$u_n^{(ZZ)}(\beta_{l,n}) = \exp \left[i \frac{\beta_{l,n}}{2} Z_n Z_{n+1} \right], \quad (18)$$

$$u_n^{(XY)}(\alpha_{l,n}) = \exp \left[i \frac{\alpha_{l,n} X_n X_{n+1} + Y_n Y_{n+1}}{2} \right]. \quad (19)$$

In the above expression L represents the depth of ansatz. Note that this ansatz preserves the global U(1) symmetry, which must be preserved for true evolution under the Hamiltonian. Note that in the following discussion the whole set of parameters is often denoted by $\boldsymbol{\lambda}$

$$\boldsymbol{\lambda} = (\boldsymbol{\alpha}_0, \boldsymbol{\beta}_0, \boldsymbol{\gamma}_0, \dots, \boldsymbol{\alpha}_{L-1}, \boldsymbol{\beta}_{L-1}, \boldsymbol{\gamma}_{L-1}),$$

and a general $u \in \{u_n^{(XY)}, u_n^{(ZZ)}, u_n^{(Z)}\}_{n=0}^{N-1}$ with dependence on these parameters is denoted by $u(\lambda)$.

B. McLachlan's variational principle

McLachlan's variational principle [100] gives the following set of equations:

$$\sum_j M_{ij} \dot{\lambda}_j = V_i, \quad (20)$$

where

$$M_{ij} = 2\text{Re}[A_{ij}] + 2C_i^{(0)} C_j^{(0)}, \quad (21)$$

$$V_i = 2\text{Im}[C_i] + 2iC_i^{(0)} \langle H \rangle_\psi, \quad (22)$$

with

$$A_{ij} = \frac{\partial \langle \psi |}{\partial \lambda_i} \frac{\partial | \psi \rangle}{\partial \lambda_j}, \quad C_i = \frac{\partial \langle \psi |}{\partial \lambda_i} H | \psi \rangle, \quad (23)$$

$$C_i^{(0)} = \frac{\partial \langle \psi |}{\partial \lambda_i} | \psi \rangle, \quad \langle H \rangle_\psi = \langle \psi | H | \psi \rangle. \quad (24)$$

Each term is evaluated on a quantum computer as follows [67]. We use the same variational ansatz used to create the ground state in the absence of the background electric field for the state after the background electric field is turned on. This allows us to obtain the corresponding ansatz for the derivatives of the state with respect to the parameters λ needed in Eqs. (23) and (24). From the explicit forms of the functions $u(\lambda)$ one obtains

$$\frac{du}{d\lambda_i} = \sum_a f_{i,a} u \sigma_{i,a}, \quad (25)$$

where $\sigma_{i,a} \in \{I, X, Y, Z\}^{\otimes N}$ and $f_{i,a}$ are complex scalar "structure constants". Explicitly the derivatives are given by

$$\frac{du_n^{(XY)}}{d\alpha_{l,n}} = \frac{i}{2} \cdot u_n^{(XY)} \frac{X_n X_{n+1} + Y_n Y_{n+1}}{2}, \quad (26)$$

$$\frac{du_n^{(ZZ)}}{d\beta_{l,n}} = \frac{i}{2} \cdot u_n^{(ZZ)} Z_n Z_{n+1}, \quad (27)$$

$$\frac{du_n^{(Z)}}{d\gamma_{l,n}} = \frac{i}{2} \cdot u_n^{(Z)} Z_n. \quad (28)$$

Using this information, one finds

$$\frac{\partial | \psi \rangle}{\partial \lambda_i} = \sum_a f_{i,a} \hat{U}_{i,a}(\lambda) | \phi \rangle, \quad (29)$$

where $\hat{U}_{i,a}(\lambda)$ is given by replacing a unitary block u corresponding to λ_i in the ansatz to $(u \sigma_{i,a})$ and $f_{i,a}$ is defined in (25). Besides, we denote the initial state as $|\phi\rangle := V_{\text{init}}|0\rangle$. Similarly, the coefficients M_{ij} and V_i given in Eqs. (21) and (22) can be evaluated as

$$M_{ij} = \frac{1}{2} \sum_{a,b} \text{Re} \left[\langle \phi | \hat{U}_{i,a}^\dagger \hat{U}_{j,b} | \phi \rangle \right] - \frac{1}{2} \sum_{a,b} \text{Re} \left[\langle \phi | \hat{U}_{i,a}^\dagger U | \phi \rangle \right] \text{Re} \left[\langle \phi | \hat{U}_{j,b}^\dagger U | \phi \rangle \right], \quad (30)$$

$$V_i = - \sum_{p,a} h_p \text{Re} \left[\langle \phi | \hat{U}_{i,a}^\dagger \sigma_p U | \phi \rangle \right] + \sum_a \text{Re} \left[\langle \phi | \hat{U}_{i,a}^\dagger U | \phi \rangle \right] \langle H \rangle_\psi. \quad (31)$$

Note that the Hamiltonian can be decomposed into Pauli strings as $H = \sum_p h_p \sigma_p$. Each term in the above equations is therefore evaluated by the quantum circuit given in Fig. 1 of [67]. The initial state in the ancilla qubit is $(|0\rangle + |1\rangle)/\sqrt{2}$ corresponding to $\theta = 0$.

Some more details on the McLachlan variational principle are given in Appendix A.

C. Quench dynamics via VQE and VQS

This section summarizes again the steps required to simulate quench dynamics using VQE and VQS variational algorithms. One starts from the ground state in the absence of the external electric field $|\Psi_{\text{GS}}(q=0)\rangle$. One then turns on the external field $q \neq 0$ and trace the time evolution, $|\Psi(t)\rangle = e^{-iH_{q \neq 0} t} |\Psi_{\text{GS}}(q=0)\rangle$.

This process is implemented through the following quantum variational protocol:

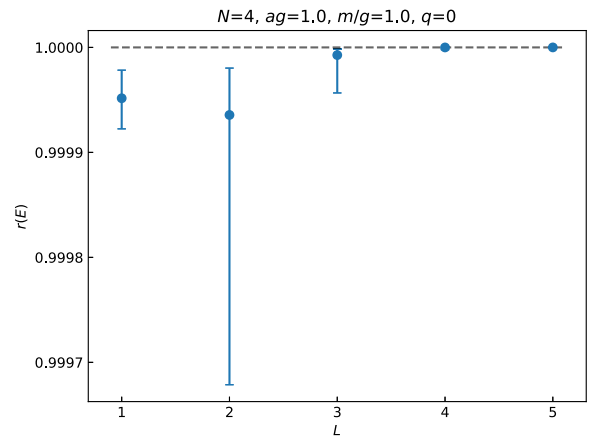


FIG. 2. Ground-state preparation via VQE: a metric of accuracy $r(E) := (E_{\text{max}} - E_{\text{VQE}})/(E_{\text{max}} - E_{\text{min}})$. Dots/error bars show the median and 25–75 percentiles of 20 samples.

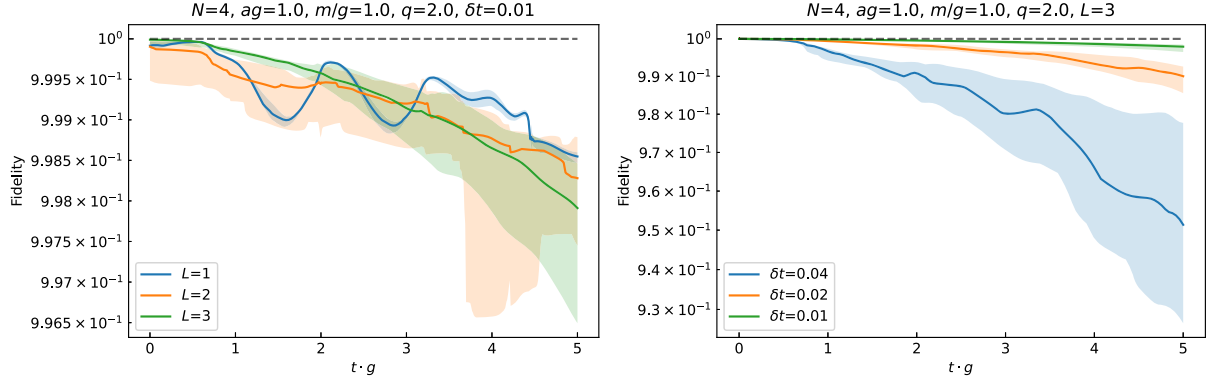


FIG. 3. Fidelity between states from VQS and ED for $N = 4$, $a \cdot g = 1.0$, $m/g = 1.0$, $q = 2.0$. Solid curves/error bands show the medians and 25–75 percentiles of 20 samples: (left) dependence of the number of layers $L \in \{1, 2, 3\}$ with $\delta t = 0.01$ fixed, (right) dependence of a time increment $\delta t \in \{0.01, 0.02, 0.04\}$ with L fixed.

- (1) State preparation via VQE: One approximates $|\Psi_{\text{GS}}(q=0)\rangle$ by $|\psi(\lambda_{\text{opt}})\rangle$, and determines λ_{opt} by minimizing $\langle \psi(\lambda) | H | \psi(\lambda) \rangle$ on a classical computer.
- (2) Real-time evolution via McLachlan’s variational principle: One uses λ_{opt} as initial values and evolve λ via (20). The coefficients M_{ij} and V_i are evaluated by a quantum circuit while the parameter evolution is done by a classical computer.

In a standard algorithm, one need both a state preparation and time-evolution circuit, but using the approach presented here one reduces the depth by using the same ansatz for both processes.

IV. RESULTS

This section presents our results of the simulation using the variational algorithms and compares them against results obtained from exact diagonalization (ED). The VQE and VQS results are obtained from noiseless state-vector simulation implemented by Qulacs [101], while ED results are obtained by QuSpin [102].

A. Ground-state preparation via VQE

We first perform VQE for $N = 4$, $ag = 1$, $m/g = 1$ in the absence of the external field $q = 0$. We repeat optimizations 20 times starting from different random initializations. Figure 2 shows a metric of accuracy [103] $r(E) := (E_{\text{max}} - E_{\text{VQE}})/(E_{\text{max}} - E_{\text{min}})$ as a function of the number of layers, where $E_{\text{max/min}}$ is the highest/lowest eigenvalue of the Hamiltonian.⁴ The central value corresponds to the median of the 20 optimizations performed, while the error bar represents the 25–75 percentiles. One observes that high-accuracy $r(E) \geq 0.999$ can be achieved for all L and that for $L \geq 4$ the uncertainties improve markedly.

⁴This ratio takes 0 for the worst case ($E_{\text{VQE}} = E_{\text{max}}$) and 1 for the best case ($E_{\text{VQE}} = E_{\text{min}}$). We obtain $E_{\text{max/min}}$ via ED.

B. Quench dynamics via VQS

After preparing the initial state, we perform VQS for $N = 4$, $ag = 1$, $m/g = 1$, and $q = 2$.⁵ First, we investigate the dependence of systematic errors on the number of layers L and a time increment δt . The left plot in Fig. 3 shows the fidelity $F(t) := |\langle \Psi_{\text{ED}}(t) | \psi_{\text{VQS}}(t) \rangle|^2$ between the states obtained from VQS and ED as a function of time (multiplied by a coupling-constant) for different number of layers. One can see that the stability improves as the number of layers is raised up to $L = 3$ and the (median) fidelity is above 0.99 for all cases. The right panel shows the same plot, but this time varying δt for fixed L . We see that the VQS results can be improved significantly by decreasing δt .

Next, we evaluate the physical observables discussed in Sec. II B and compare them to the results obtained by exact diagonalization. We verified that the U(1) charge agrees perfectly with the exact result, as can be expected since our ansatz satisfies the global U(1) symmetry of the problem. The remaining two observables are shown in Fig. 4 with $L = 3$ and $\delta t = 0.01$ fixed. The VQS results are consistent with those from ED up to a few % errors. The errors from the variation over the 20 initial conditions is of the same order of magnitude as the difference from the exact result, but for the electric field and $1.5 \lesssim t \cdot g \lesssim 4.5$ the difference between the exact result and the central value of the VQS results are about three times the size of the quoted error.

For $t \cdot g \lesssim 3$, the value of the electric field decreases while that of the chiral condensate increases, followed by the oscillation. This can be interpreted as follows—the external electric field first provides energy for fermions and then leads to particle-pair creations.

Finally, let us comment on the scaling of the variational methods. It is very important to understand how the errors/resources scale with the lattice size/spacing, since we are

⁵We regularize the matrix M_{ij} as $M \rightarrow M + \epsilon I$ if $\det(M) < \epsilon$ when we perform a matrix inversion. In the following simulation, we set $\epsilon = 10^{-7}$.

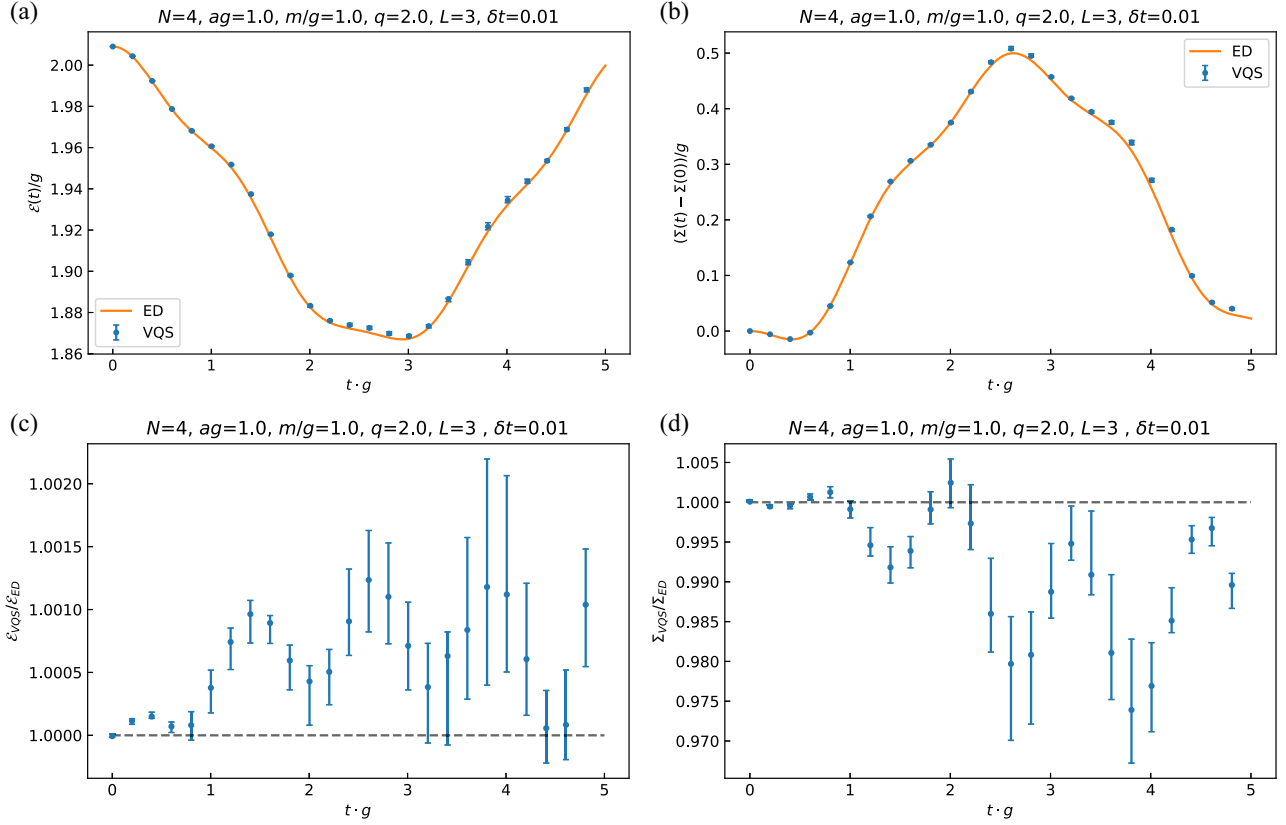


FIG. 4. Dynamics of physical observables for $N = 4$, $a \cdot g = 1.0$, $m/g = 1.0$, $q = 2.0$ with $L = 3$ and $\delta = 0.01$. Dots/error bars show the median and 25–75 percentiles of 20 samples: (a) electric field, (b) chiral condensate, (c), (d) ratio between the values of observables obtained from ED and VQS.

eventually interested in continuum and infinite volume limit. We provide additional results in Appendix B to show the dependence of accuracy on the system size and lattice spacing. As for system-size dependence, we observe that the accuracy gets worse with increasing N , though we can achieve $F > 0.9$ at least up to $N = 8$ only with $L \leq 3$. Further investigation of the scaling would require the large size simulation possibly with improved algorithms, which we leave for the future works.

V. SUMMARY AND DISCUSSION

In this work, we demonstrated a possible application of the variational quantum algorithm to a gauge theory. Specifically, we investigated the real-time dynamics in the Schwinger model after suddenly turning on the external electric field, by combining VQE and VQS methods. We performed the (classically-emulated) state-vector simulation and found that the results obtained from the quantum algorithms are consistent with those obtained from ED. Our simulation results can be interpreted as a population of a particle-antiparticle pair induced by the external field.

There are many possible future directions. This paper used the original algorithm proposed by Li and Benjamin [66].

There are two main drawbacks to this approach: First, the matrix M can be singular or ill-conditioned in practice, leading to unstable trajectories. Workarounds such as regularization add a parameter that must be tuned. Secondly, computing the each entry of M requires $O(N_p^2)$ calls to the quantum computer where N_p is the number of parameters. There are many attempts to overcome this problem [71–83]. It would be important to see if these methods can improve our simulation results in terms of accuracy and measurement cost.

Toward an implementation on real quantum devices, it is important to understand the effects of hardware noise and statistical error coming from a finite number of measurements. Besides, combination with error mitigation methods can be an essential ingredient.

Finally, it would be interesting to consider an extension to the higher-dimensional and/or non-Abelian gauge theory. For this purpose, a careful search for an ansatz that is efficient and preserves gauge invariance during simulation can be crucial.

ACKNOWLEDGMENTS

L. N. would like to thank N. Gomes and M. Honda for useful conversations. He would also like to thank H. Taya

for his seminar on the Schwinger mechanism. This study is partly carried out under the project ‘‘Optimization of HEP Quantum Algorithms’’ supported by the U.S.-Japan Science and Technology Cooperation Program in High Energy Physics. C. W. B. and A. B. also acknowledge support from the DOE, Office of Science under Contract No. DE-AC02-05CH11231, through Quantum Information Science Enabled Discovery (QuantISED) for High Energy Physics (KA2401032).

APPENDIX A: McLACHLAN’S VARIATIONAL PRINCIPLE

This variational principle starts from a variational ansatz state $|\psi(\lambda)\rangle$ given as the output of a parametrized circuit (and a global phase λ_0),

$$|\psi(\lambda)\rangle = e^{i\lambda_0(t)} \prod_{i=1}^{N_p} U(\lambda_i(t))|0\rangle. \quad (\text{A1})$$

In other words, the time dependence of the state is encoded through the time dependence of the parameters $\lambda(t)$.

The task of simulating Schrödinger evolution $|\Psi(t)\rangle = \mathcal{T}e^{-i\int H(s)ds}|\Psi(0)\rangle$ under a general, time-dependent Hamiltonian $H(t)$ using the ansatz state $|\psi(\lambda)\rangle$ reduces to finding the parameter function $\lambda(t)$ such that at any time t , the state $|\psi(\lambda(t))\rangle$ optimally approximates the exact state $|\Psi(t)\rangle$.

A standard approach to this problem is to use a dynamical variational principle such as the McLachlan’s variational principle, or MVP for short. Other choices such as the Dirac-Frenkel variational principle and the time-dependent variational principle exist, and while different in subtle ways, they all agree under certain mild assumptions. In this section we focus on the MVP.

The central idea behind MVP is to minimize the difference between the rates of change of $|\psi\rangle$ under exact Hamiltonian evolution and variational evolution due to $d\lambda/dt$. Normally, this is expressed as minimizing the variation of the norm difference shown below,

$$\delta \left\| \left(\frac{d}{dt} + iH \right) |\psi(\lambda(t))\rangle \right\|^2 = 0, \quad (\text{A2})$$

where $\|\cdot\|$ is the l_2 -norm. Note that the variation in the above is with respect to $\delta(d\lambda_i/dt)$, i.e., total time derivatives in each parameter λ_i . In other words, one is looking for stationary points by varying the tangent vector $d\lambda/dt$. Since one is dealing with a time-dependent Hamiltonian, the equation has to be written a little more carefully as

$$\lim_{\Delta t \rightarrow 0} \delta \frac{\|(U(t + \Delta t, t) - I)|\psi\rangle - \Delta t|\dot{\psi}\rangle\|^2}{\Delta t^2} = 0, \quad (\text{A3})$$

where $U(t', t) := \mathcal{T}e^{-i\int_t^{t'} H(s)ds}$ and I is the identity matrix. The main difference from the time-independent case is due to the appearance of an extra term at order Δt^2 due to the time dependence of H ,

$$U(t + \Delta t, t) = I - iH\Delta t - (H^2 + i\dot{H})\frac{\Delta t^2}{2} + O(\Delta t^3) \quad (\text{A4})$$

$$\equiv U_{TI}(t + \Delta t, t) - i\dot{H}\frac{\Delta t^2}{2} + O(\Delta t^3), \quad (\text{A5})$$

where U_{TI} is the propagator if H were held constant in time at the value $H(t)$. However, since the limit is insensitive to terms above linear order, the time dependence of H can be safely ignored.

Before expanding (A2), one can implement some constraints on $|\psi\rangle$ and its time derivatives due to the normalization condition $\langle\psi|\psi\rangle = 1$. Setting the first and second time derivatives to zero yields, respectively,

$$\langle\dot{\psi}|\psi\rangle = -\langle\psi|\dot{\psi}\rangle, \quad (\text{A6})$$

$$\text{Re}\langle\ddot{\psi}|\psi\rangle = -\langle\dot{\psi}|\dot{\psi}\rangle. \quad (\text{A7})$$

Now, one expands the norm of the difference vector,

$$\|(\dot{\psi} + iH|\psi)\|^2 = (\langle\dot{\psi}| - i\langle\psi|H)(|\dot{\psi}\rangle + iH|\psi\rangle) \quad (\text{A8})$$

$$= \langle\dot{\psi}|\dot{\psi}\rangle - 2\text{Im}\langle\psi|H|\dot{\psi}\rangle + \langle H^2\rangle, \quad (\text{A9})$$

using the notation $\langle O\rangle = \langle\psi|O|\psi\rangle$. Next, one writes $|\dot{\psi}\rangle$ in terms of partial derivatives

$$|\dot{\psi}\rangle = \dot{\lambda}_0 \frac{\partial}{\partial \lambda_0} |\psi\rangle + \sum_{i=1}^{N_p} \dot{\lambda}_i \frac{\partial}{\partial \lambda_i} |\psi\rangle = i\dot{\lambda}_0 |\psi\rangle + \dot{\lambda}_i |\partial_i \psi\rangle, \quad (\text{A10})$$

where $|\partial_i \psi\rangle = \frac{\partial}{\partial \lambda_i} |\psi\rangle$. The last expression is implicitly summed over i from 1 to N_p , and the $i=0$ term (corresponding to global phase) gives a derivative parallel to $|\psi\rangle$. The purpose of the λ_0 term is to keep track of variations parallel to ψ which do not change the overall state but can have an effect on the dynamics of the variational parameters. In practice, including it can lead to more well-behaved dynamics.

Then, one can separately express the terms containing $|\dot{\psi}\rangle$ as

$$\langle\dot{\psi}|\dot{\psi}\rangle = \dot{\lambda}_i \dot{\lambda}_j \text{Re}\langle\partial_i \psi|\partial_j \psi\rangle + \dot{\lambda}_0 \dot{\lambda}_i \text{Im}\langle\psi|\partial_i \psi\rangle + \dot{\lambda}_0^2, \quad (\text{A11})$$

$$\text{Im}\langle\psi|H|\dot{\psi}\rangle = \dot{\lambda}_0 \langle H\rangle + \dot{\lambda}_i \text{Im}\langle\psi|H|\partial_i \psi\rangle, \quad (\text{A12})$$

where the properties $\langle\psi|\psi\rangle = 1$ and $\langle\psi|H|\psi\rangle = \langle H\rangle$ is real have been used. Taken together, this yields

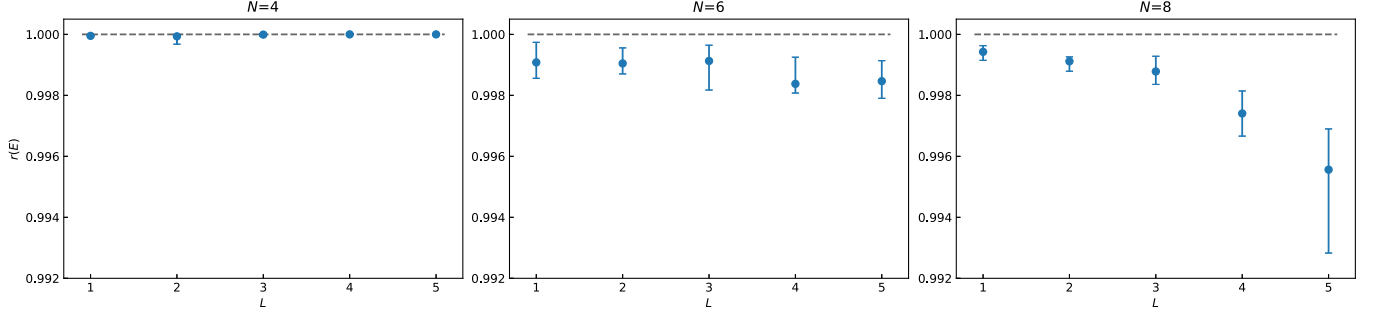


FIG. 5. Dependence of VQE accuracy $r(E)$ on system size N . Three panels show the results for $N = 4, 6, 8$ respectively with $ag = 1.0$, $m/g = 1.0$ fixed. Dots/error bars show the median and 25–75 percentiles of 20 samples.

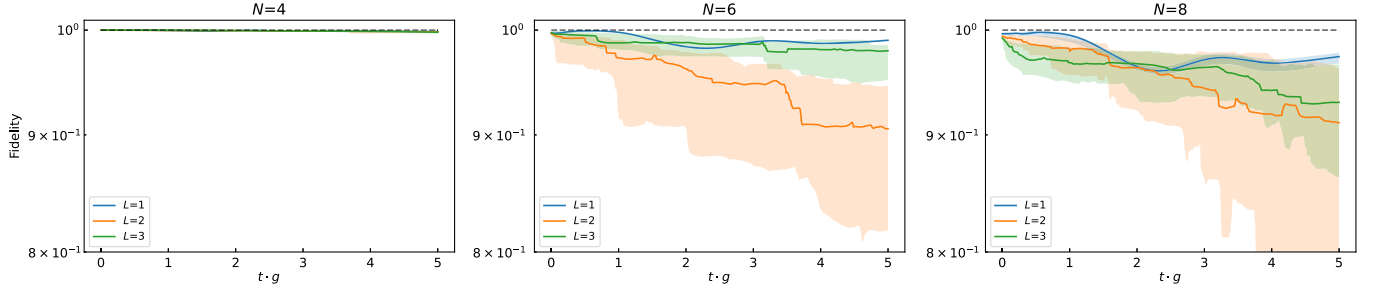


FIG. 6. Dependence of VQS fidelity on system size N . Three panels show the results for $N = 4, 6, 8$ respectively. Each panel shows results with various depths $L = 1, 2, 3$ while $a \cdot g = 1.0$, $m/g = 1.0$, $q = 2.0$ are fixed. Solid curves/error bands show the medians and 25–75 percentiles of 20 samples.

$$\begin{aligned} \|\dot{\psi} + iH\psi\|^2 &= \dot{\lambda}_i \dot{\lambda}_j \text{Re}\langle \partial_i \psi | \partial_j \psi \rangle + \dot{\lambda}_0 \dot{\lambda}_i \text{Im}\langle \psi | \partial_i \psi \rangle \\ &\quad + \dot{\lambda}_0^2 - 2\dot{\lambda}_0 \langle H \rangle - 2\dot{\lambda}_i \text{Im}\langle \psi | H | \partial_i \psi \rangle \\ &\quad + \langle H^2 \rangle, \end{aligned} \quad (\text{A13})$$

$$\begin{aligned} &= \dot{\lambda}_i \dot{\lambda}_j \text{Re}\langle \partial_i \psi | \partial_j \psi \rangle + \dot{\lambda}_0 \dot{\lambda}_i \text{Im}\langle \psi | \partial_i \psi \rangle \\ &\quad - 2\dot{\lambda}_i \text{Im}\langle \psi | H | \partial_i \psi \rangle + (\dot{\lambda}_0 - \langle H \rangle)^2 \\ &\quad + \sigma_{\dot{\psi}}^2(H), \end{aligned} \quad (\text{A14})$$

where $\sigma_{\dot{\psi}}^2(H) := \langle H^2 \rangle - \langle H \rangle^2$ is the variance of H in the state $|\psi\rangle$. Now one derives stationary conditions by setting the derivatives in $\dot{\lambda}_0$ and each $\dot{\lambda}_i$ to 0. The first condition gives

$$\dot{\lambda}_0 = \langle H \rangle + \dot{\lambda}_i \text{Im}\langle \psi | \partial_i \psi \rangle, \quad (\text{A15})$$

while the remaining conditions in each i are given by

$$\dot{\lambda}_j \text{Re}\langle \partial_i \psi | \partial_j \psi \rangle + \dot{\lambda}_0 \text{Im}\langle \psi | \partial_i \psi \rangle - \text{Im}\langle \psi | H | \partial_i \psi \rangle = 0. \quad (\text{A16})$$

Substituting for $\dot{\lambda}_0$, and defining the projection operators $Q_{\psi} := I - |\psi\rangle\langle\psi| = I - P_{\psi}$, one arrives at the final expression

$$(\text{Re}\langle \partial_i \psi | Q_{\psi} | \partial_j \psi \rangle) \dot{\lambda}_j = (\text{Im}\langle \psi | H Q_{\psi} | \partial_i \psi \rangle). \quad (\text{A17})$$

The matrix $M_{ij} := \text{Re}\langle \partial_i \psi | Q_{\psi} | \partial_j \psi \rangle$ and vector $V_i := \text{Im}\langle \psi | H Q_{\psi} | \partial_i \psi \rangle$ specify a linear system whose solutions give

the McLachlan update vectors $\dot{\lambda}_i$ in each direction. Note that, while trivial, the global-phase evolution can also be tracked via (A15).

APPENDIX B: DEPENDENCE ON LATTICE SIZE/SPACING

In this appendix we provide additional plots to show the dependence of VQE and VQS on a lattice spacing a and a system size N .

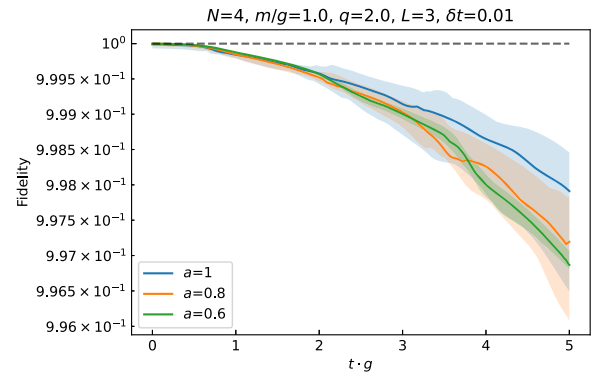


FIG. 7. Dependence of VQS fidelity on lattice spacing a . Results for $a = 1, 0.8, 0.6$ with $N = 4$, $m/g = 1.0$, $q = 2.0$, $L = 3$ fixed are shown. Solid curves/error bands show the medians and 25–75 percentiles of 20 samples.

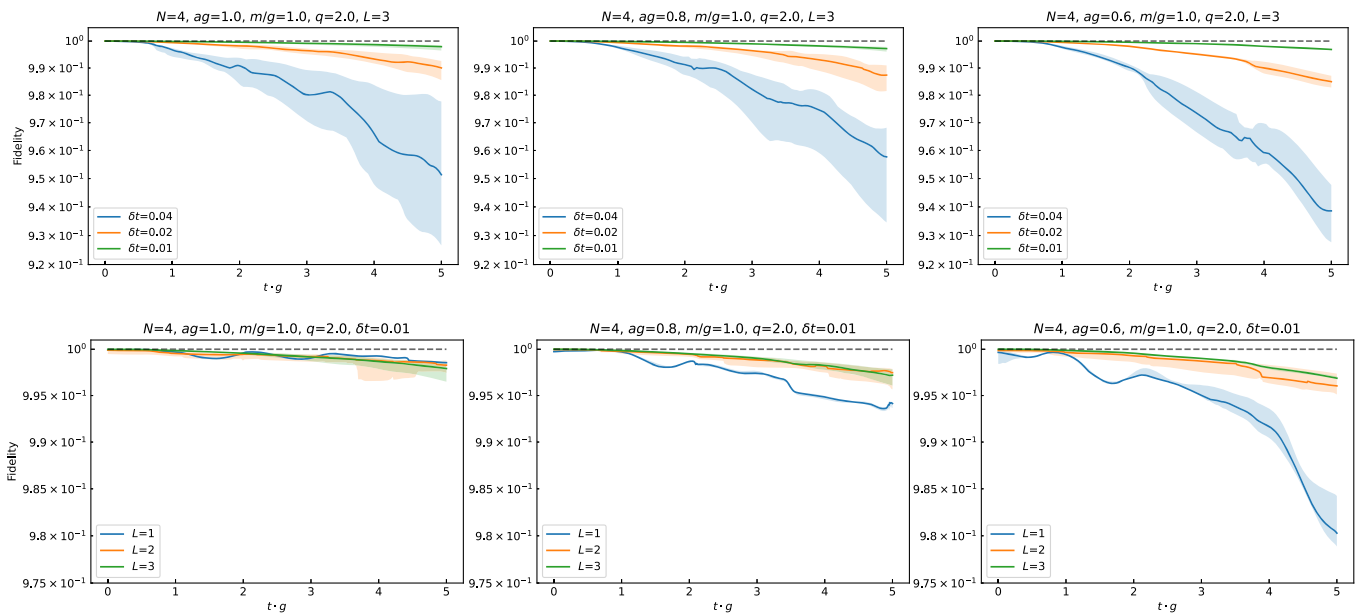


FIG. 8. Dependence of VQS fidelity on lattice spacing a with $N = 4$, $m/g = 1.0$, $q = 2.0$ fixed. Top panels show the δt dependence with $L = 3$ fixed, while bottom show the L dependence with $\delta t = 0.01$ fixed. Solid curves/error bands show the medians and 25–75 percentiles of 20 samples.

First, let us investigate the system size dependence. Figure 5 shows the N -dependence of the accuracy $r(E)$ for VQE. We see that the accuracy gets worse with increasing N , though we can achieve $r(E) > 0.99$ for $N \leq 8$ with $L = 5$. We then plot the fidelity F of the VQS simulation for $N = 4, 6, 8$ in Fig. 6. As expected naively, the fidelity for $N = 6, 8$ are worse than that for $N = 4$. Nevertheless, we can achieve $F > 0.9$ using the ansatz with $L \leq 3$ at least up to $N = 8$. It would be important to investigate further the

scaling of the minimal number of depth L to achieve certain accuracy with increasing system sizes.

Next, we consider the lattice spacing dependence. Figure 7 shows the fidelity of VQS simulation with varying the value of a . We see that the fidelity gets worse for smaller a , but the effects are not significant at least for $N = 4$. As seen from Fig. 8, one can improve the accuracy by increasing the number of steps, while increasing the number of depths does not lead to significant improvement.

-
- [1] S. P. Jordan, K. S. M. Lee, and J. Preskill, Quantum algorithms for quantum field theories, *Science* **336**, 1130 (2012).
 - [2] S. P. Jordan, K. S. M. Lee, and J. Preskill, Quantum computation of scattering in scalar quantum field theories, *Quantum Inf. Comput.* **14**, 1014 (2014).
 - [3] S. P. Jordan, K. S. M. Lee, and J. Preskill, Quantum algorithms for fermionic quantum field theories, [arXiv:1404.7115](https://arxiv.org/abs/1404.7115).
 - [4] E. A. Martinez *et al.*, Real-time dynamics of lattice gauge theories with a few-qubit quantum computer, *Nature (London)* **534**, 516 (2016).
 - [5] C. Muschik, M. Heyl, E. Martinez, T. Monz, P. Schindler, B. Vogell, M. Dalmonte, P. Hauke, R. Blatt, and P. Zoller, U(1) Wilson lattice gauge theories in digital quantum simulators, *New J. Phys.* **19**, 103020 (2017).
 - [6] N. Klco, E. F. Dumitrescu, A. J. McCaskey, T. D. Morris, R. C. Pooser, M. Sanz, E. Solano, P. Lougovski, and M. J. Savage, Quantum-classical computation of Schwinger model dynamics using quantum computers, *Phys. Rev. A* **98**, 032331 (2018).
 - [7] C. Kokail *et al.*, Self-verifying variational quantum simulation of lattice models, *Nature (London)* **569**, 355 (2019).
 - [8] G. Magnifico, M. Dalmonte, P. Facchi, S. Pascazio, F. V. Pepe, and E. Ercolessi, Real time dynamics and confinement in the \mathbb{Z}_n Schwinger-Weyl lattice model for $1 + 1$ QED, *Quantum* **4**, 281 (2020).
 - [9] B. Chakraborty, M. Honda, T. Izubuchi, Y. Kikuchi, and A. Tomiya, Classically emulated digital quantum simulation of the Schwinger model with a topological term via adiabatic state preparation, *Phys. Rev. D* **105**, 094503 (2022).
 - [10] M. Honda, E. Itou, Y. Kikuchi, L. Nagano, and T. Okuda, Classically emulated digital quantum simulation for screening and confinement in the Schwinger model with a topological term, *Phys. Rev. D* **105**, 014504 (2022).

- [11] M. Honda, E. Itou, Y. Kikuchi, and Y. Tanizaki, Negative string tension of a higher-charge Schwinger model via digital quantum simulation, *Prog. Theor. Exp. Phys.* **2022**, 033B01 (2022).
- [12] W. A. de Jong, K. Lee, J. Mulligan, M. Płoskoń, F. Ringer, and X. Yao, Quantum simulation of non-equilibrium dynamics and thermalization in the Schwinger model, *Phys. Rev. D* **106**, 054508 (2022).
- [13] A. Yamamoto, Quantum variational approach to lattice gauge theory at nonzero density, *Phys. Rev. D* **104**, 014506 (2021).
- [14] D. E. Kharzeev and Y. Kikuchi, Real-time chiral dynamics from a digital quantum simulation, *Phys. Rev. Res.* **2**, 023342 (2020).
- [15] E. Gustafson, P. Dreher, Z. Hang, and Y. Meurice, Real time evolution of a one-dimensional field theory on a 20 qubit machine, *Quantum Sci. Technol.* **6**, 045020 (2021).
- [16] E. J. Gustafson and H. Lamm, Toward quantum simulations of Z_2 gauge theory without state preparation, *Phys. Rev. D* **103**, 054507 (2021).
- [17] A. F. Shaw, P. Lougovski, J. R. Stryker, and N. Wiebe, Quantum algorithms for simulating the lattice Schwinger model, *Quantum* **4**, 306 (2020).
- [18] D. Banerjee, S. Caspar, F.-J. Jiang, J.-H. Peng, and U.-J. Wiese, Nematic confined phases in the $U(1)$ quantum link model on a triangular lattice: Near-term quantum computations of string dynamics on a chip, *Phys. Rev. Res.* **4**, 023176 (2022).
- [19] X.-D. Xie, X. Guo, H. Xing, Z.-Y. Xue, D.-B. Zhang, and S.-L. Zhu (QuNu Collaboration), Variational thermal quantum simulation of the lattice Schwinger model, *Phys. Rev. D* **106**, 054509 (2022).
- [20] N. H. Nguyen, M. C. Tran, Y. Zhu, A. M. Green, C. H. Alderete, Z. Davoudi, and N. M. Linke, Digital quantum simulation of the Schwinger model and symmetry protection with trapped ions, *PRX Quantum* **3**, 020324 (2022).
- [21] A. Tomiya, Schwinger model at finite temperature and density with beta VQE, [arXiv:2205.08860](https://arxiv.org/abs/2205.08860).
- [22] J. Mildenerger, W. Mruczkiewicz, J. C. Halimeh, Z. Jiang, and P. Hauke, Probing confinement in a Z_2 lattice gauge theory on a quantum computer, [arXiv:2203.08905](https://arxiv.org/abs/2203.08905).
- [23] A. N. Ciavarella and I. A. Chernyshev, Preparation of the $SU(3)$ lattice Yang-Mills vacuum with variational quantum methods, *Phys. Rev. D* **105**, 074504 (2022).
- [24] Y. Atas, J. Zhang, R. Lewis, A. Jahanpour, J. F. Haase, and C. A. Muschik, $SU(2)$ hadrons on a quantum computer, *Nat. Commun.* **12**, 6499 (2021).
- [25] Y. Y. Atas, J. F. Haase, J. Zhang, V. Wei, S. M. L. Pfaendler, R. Lewis, and C. A. Muschik, Real-time evolution of $SU(3)$ hadrons on a quantum computer, [arXiv:2207.03473](https://arxiv.org/abs/2207.03473).
- [26] A. Mezzacapo, E. Rico, C. Sabin, I. L. Egusquiza, L. Lamata, and E. Solano, Non-Abelian $SU(2)$ Lattice Gauge Theories in Superconducting Circuits, *Phys. Rev. Lett.* **115**, 240502 (2015).
- [27] D. Marcos, P. Widmer, E. Rico, M. Hafezi, P. Rabl, U. J. Wiese, and P. Zoller, Two-dimensional lattice gauge theories with superconducting quantum circuits, *Ann. Phys. (Amsterdam)* **351**, 634 (2014).
- [28] N. Klco, J. R. Stryker, and M. J. Savage, $SU(2)$ non-Abelian gauge field theory in one dimension on digital quantum computers, *Phys. Rev. D* **101**, 074512 (2020).
- [29] A. Ciavarella, N. Klco, and M. J. Savage, Trailhead for quantum simulation of $SU(3)$ Yang-Mills lattice gauge theory in the local multiplet basis, *Phys. Rev. D* **103**, 094501 (2021).
- [30] G. Clemente, A. Crippa, and K. Jansen, Strategies for the determination of the running coupling of $(2+1)$ -dimensional QED with quantum computing, *Phys. Rev. D* **106**, 114511 (2022).
- [31] C. Kane, D. M. Grabowska, B. Nachman, and C. W. Bauer, Efficient quantum implementation of $2+1$ $U(1)$ lattice gauge theories with Gauss law constraints, [arXiv:2211.10497](https://arxiv.org/abs/2211.10497).
- [32] L. Lumia, P. Torta, G. B. Mbeng, G. E. Santoro, E. Ercolessi, M. Burrello, and M. M. Wauters, Two-dimensional z_2 lattice gauge theory on a near-term quantum simulator: Variational quantum optimization, confinement, and topological order, *PRX Quantum* **3**, 020320 (2022).
- [33] D. Paulson, L. Dellantonio, J. F. Haase, A. Celi, A. Kan, A. Jena, C. Kokail, R. van Bijnen, K. Jansen, P. Zoller, and C. A. Muschik, Simulating 2D effects in lattice gauge theories on a quantum computer, *PRX Quantum* **2**, 030334 (2021).
- [34] E. Huffman, M. García Vera, and D. Banerjee, Toward the real-time evolution of gauge-invariant z_2 and $U(1)$ quantum link models on noisy intermediate-scale quantum hardware with error mitigation, *Phys. Rev. D* **106**, 094502 (2022).
- [35] N. Klco and M. J. Savage, Digitization of scalar fields for quantum computing, *Phys. Rev. A* **99**, 052335 (2019).
- [36] J. Barata, N. Mueller, A. Tarasov, and R. Venugopalan, Single-particle digitization strategy for quantum computation of a ϕ^4 scalar field theory, *Phys. Rev. A* **103**, 042410 (2021).
- [37] L. Garcia-Alvarez, J. Casanova, A. Mezzacapo, I. L. Egusquiza, L. Lamata, G. Romero, and E. Solano, Fermion-Fermion Scattering in Quantum Field Theory with Superconducting Circuits, *Phys. Rev. Lett.* **114**, 070502 (2015).
- [38] U.-J. Wiese, Towards quantum simulating QCD, *Nucl. Phys.* **A931**, 246 (2014).
- [39] E. Gustafson, Y. Meurice, and J. Unmuth-Yockey, Quantum simulation of scattering in the quantum Ising model, *Phys. Rev. D* **99**, 094503 (2019).
- [40] A. Kan and Y. Nam, Lattice quantum chromodynamics and electrodynamics on a universal quantum computer, [arXiv:2107.12769](https://arxiv.org/abs/2107.12769).
- [41] G. Pardo, T. Greenberg, A. Fortinsky, N. Katz, and E. Zohar, Resource-efficient quantum simulation of lattice gauge theories in arbitrary dimensions: Solving for Gauss' law and fermion elimination, *Phys. Rev. Res.* **5**, 023077 (2023).
- [42] E. J. Gustafson, Stout smearing on a quantum computer, [arXiv:2211.05607](https://arxiv.org/abs/2211.05607).
- [43] M. G. Echevarria, I. L. Egusquiza, E. Rico, and G. Schnell, Quantum simulation of light-front parton correlators, *Phys. Rev. D* **104**, 014512 (2021).

- [44] Y. Su, H.-Y. Huang, and E. T. Campbell, Nearly tight trotterization of interacting electrons, *Quantum* **5**, 495 (2021).
- [45] J. Liu and Y. Xin, Quantum simulation of quantum field theories as quantum chemistry, *J. High Energy Phys.* **12** (2020) 011.
- [46] A. J. Buser, H. Gharibyan, M. Hanada, M. Honda, and J. Liu, Quantum simulation of gauge theory via orbifold lattice, *J. High Energy Phys.* **09** (2021) 034.
- [47] N. Klco and M. J. Savage, Fixed-point quantum circuits for quantum field theories, *Phys. Rev. A* **102**, 052422 (2020).
- [48] N. Klco and M. J. Savage, Minimally-entangled state preparation of localized wavefunctions on quantum computers, *Phys. Rev. A* **102**, 012612 (2020).
- [49] M. Asaduzzaman, G. C. Toga, S. Catterall, Y. Meurice, and R. Sakai, Quantum simulation of the n -flavor Gross-Neveu model, *Phys. Rev. D* **106**, 114515 (2022).
- [50] Z. Davoudi, A. F. Shaw, and J. R. Stryker, General quantum algorithms for Hamiltonian simulation with applications to a non-Abelian lattice gauge theory, [arXiv:2212.14030](https://arxiv.org/abs/2212.14030).
- [51] Z. Davoudi, I. Raychowdhury, and A. Shaw, Search for efficient formulations for Hamiltonian simulation of non-Abelian lattice gauge theories, *Phys. Rev. D* **104**, 074505 (2021).
- [52] Z. Davoudi, N. Mueller, and C. Powers, Toward quantum computing phase diagrams of gauge theories with thermal pure quantum states, [arXiv:2208.13112](https://arxiv.org/abs/2208.13112).
- [53] J. R. Stryker, Shearing approach to gauge invariant trotterization, [arXiv:2105.11548](https://arxiv.org/abs/2105.11548).
- [54] A. Yamamoto and T. Doi, Toward nuclear physics from lattice QCD on quantum computers, [arXiv:2211.14550](https://arxiv.org/abs/2211.14550).
- [55] C. W. Bauer, B. Nachman, and M. Freytsis, Simulating Collider Physics on Quantum Computers Using Effective Field Theories, *Phys. Rev. Lett.* **127**, 212001 (2021).
- [56] J. Liu and Y.-Z. Li, Quantum simulation of cosmic inflation, *Phys. Rev. D* **104**, 086013 (2021).
- [57] H. Gharibyan, M. Hanada, M. Honda, and J. Liu, Toward simulating superstring/M-theory on a quantum computer, *J. High Energy Phys.* **07** (2021) 140.
- [58] F. Mei, Q. Guo, Y.-F. Yu, L. Xiao, S.-L. Zhu, and S. Jia, Digital Simulation of Topological Matter on Programmable Quantum Processors, *Phys. Rev. Lett.* **125**, 160503 (2020).
- [59] F. Arute *et al.*, Observation of separated dynamics of charge and spin in the Fermi-Hubbard model, [arXiv:2010.07965](https://arxiv.org/abs/2010.07965).
- [60] H. Lamm, S. Lawrence, and Y. Yamauchi (NuQS Collaboration), Parton physics on a quantum computer, *Phys. Rev. Res.* **2**, 013272 (2020).
- [61] N. Mueller, A. Tarasov, and R. Venugopalan, Deeply inelastic scattering structure functions on a hybrid quantum computer, *Phys. Rev. D* **102**, 016007 (2020).
- [62] A. J. Buser, T. Bhattacharya, L. Cincio, and R. Gupta, State preparation and measurement in a quantum simulation of the O(3) sigma model, *Phys. Rev. D* **102**, 114514 (2020).
- [63] H. Lamm and S. Lawrence, Simulation of Nonequilibrium Dynamics on a Quantum Computer, *Phys. Rev. Lett.* **121**, 170501 (2018).
- [64] A. Alexandru, P. F. Bedaque, H. Lamm, and S. Lawrence (NuQS Collaboration), σ Models on Quantum Computers, *Phys. Rev. Lett.* **123**, 090501 (2019).
- [65] A. Macridin, P. Spentzouris, J. Amundson, and R. Harnik, Electron-Phonon Systems on a Universal Quantum Computer, *Phys. Rev. Lett.* **121**, 110504 (2018).
- [66] Y. Li and S. C. Benjamin, Efficient Variational Quantum Simulator Incorporating Active Error Minimization, *Phys. Rev. X* **7**, 021050 (2017).
- [67] X. Yuan, S. Endo, Q. Zhao, Y. Li, and S. C. Benjamin, Theory of variational quantum simulation, *Quantum* **3**, 191 (2019).
- [68] S. Endo, J. Sun, Y. Li, S. C. Benjamin, and X. Yuan, Variational Quantum Simulation of General Processes, *Phys. Rev. Lett.* **125**, 010501 (2020).
- [69] S. Endo, I. Kurata, and Y. O. Nakagawa, Calculation of the Green's function on near-term quantum computers, *Phys. Rev. Res.* **2**, 033281 (2020).
- [70] Y.-X. Yao, N. Gomes, F. Zhang, C.-Z. Wang, K.-M. Ho, T. Iadecola, and P. P. Orth, Adaptive variational quantum dynamics simulations, *PRX Quantum* **2**, 030307 (2021).
- [71] C. Cîrstoiu, Z. Holmes, J. Iosue, L. Cincio, P. J. Coles, and A. Sornborger, Variational fast forwarding for quantum simulation beyond the coherence time, *npj Quantum Inf.* **6**, 82 (2020).
- [72] J. Gibbs, K. Gili, Z. Holmes, B. Commeau, A. Arrasmith, L. Cincio, P. J. Coles, and A. Sornborger, Long-time simulations for fixed input states on quantum hardware, *npj Quantum Inf.* **8**, 135 (2022).
- [73] B. Commeau, M. Cerezo, Z. Holmes, L. Cincio, P. J. Coles, and A. Sornborger, Variational Hamiltonian diagonalization for dynamical quantum simulation, [arXiv:2009.02559](https://arxiv.org/abs/2009.02559).
- [74] M. Benedetti, M. Fiorentini, and M. Lubasch, Hardware-efficient variational quantum algorithms for time evolution, *Phys. Rev. Res.* **3**, 033083 (2021).
- [75] S.-H. Lin, R. Dilip, A. G. Green, A. Smith, and F. Pollmann, Real- and imaginary-time evolution with compressed quantum circuits, *PRX Quantum* **2**, 010342 (2021).
- [76] F. Barratt, J. Dborin, M. Bal, V. Stojevic, F. Pollmann, and A. G. Green, Parallel quantum simulation of large systems on small NISQ computers, *npj Quantum Inf.* **7**, 79 (2021).
- [77] S. Barison, F. Vicentini, and G. Carleo, An efficient quantum algorithm for the time evolution of parameterized circuits, *Quantum* **5**, 512 (2021).
- [78] K. Heya, K. M. Nakanishi, K. Mitarai, and K. Fujii, Subspace variational quantum simulator, *Phys. Rev. Res.* **5**, 023078 (2023).
- [79] L. Slattery, B. Villalonga, and B. K. Clark, Unitary block optimization for variational quantum algorithms, *Phys. Rev. Res.* **4**, 023072 (2022).
- [80] K. Bharti and T. Haug, Quantum-assisted simulator, *Phys. Rev. A* **104**, 042418 (2021).
- [81] J. W. Z. Lau, K. Bharti, T. Haug, and L. C. Kwek, Noisy intermediate scale quantum simulation of time dependent Hamiltonians, [arXiv:2101.07677](https://arxiv.org/abs/2101.07677).
- [82] J. W. Z. Lau, T. Haug, L. C. Kwek, and K. Bharti, NISQ algorithm for Hamiltonian simulation via truncated Taylor series, *SciPost Phys.* **12**, 122 (2022).

- [83] S. Barison, F. Vicentini, I. Cirac, and G. Carleo, Variational dynamics as a ground-state problem on a quantum computer, *Phys. Rev. Res.* **4**, 043161 (2022).
- [84] K. Wada, R. Raymond, Y.-y. Ohnishi, E. Kaminishi, M. Sugawara, N. Yamamoto, and H. C. Watanabe, Simulating time evolution with fully optimized single-qubit gates on parametrized quantum circuits, *Phys. Rev. A* **105**, 062421 (2022).
- [85] A. Miessen, P. J. Ollitrault, F. Tacchino, and I. Tavernelli, Quantum algorithms for quantum dynamics, NATO ASI series Series F, Computer and system sciences **3**, 25 (2023).
- [86] J. Liu, Z. Li, H. Zheng, X. Yuan, and J. Sun, Towards a variational Jordan-Lee-Preskill quantum algorithm, *Mach. Learn.* **3**, 045030 (2022).
- [87] J. Schwinger, On gauge invariance and vacuum polarization, *Phys. Rev.* **82**, 664 (1951).
- [88] B. Buyens, J. Haegeman, F. Hebenstreit, F. Verstraete, and K. Van Acoleyen, Real-time simulation of the Schwinger effect with matrix product states, *Phys. Rev. D* **96**, 114501 (2017).
- [89] B. Xu and W. Xue, $(3 + 1)$ -dimensional Schwinger pair production with quantum computers, *Phys. Rev. D* **106**, 116007 (2022).
- [90] J. S. Schwinger, Gauge invariance and mass. 2., *Phys. Rev.* **128**, 2425 (1962).
- [91] J. Lowenstein and J. Swieca, Quantum electrodynamics in two dimensions, *Ann. Phys. (N.Y.)* **68**, 172 (1971).
- [92] S. R. Coleman, R. Jackiw, and L. Susskind, Charge shielding and quark confinement in the massive Schwinger model, *Ann. Phys. (N.Y.)* **93**, 267 (1975).
- [93] D. J. Gross, I. R. Klebanov, A. V. Matytsin, and A. V. Smilga, Screening versus confinement in $(1 + 1)$ -dimensions, *Nucl. Phys.* **B461**, 109 (1996).
- [94] J. B. Kogut and L. Susskind, Hamiltonian formulation of Wilson's lattice gauge theories, *Phys. Rev. D* **11**, 395 (1975).
- [95] P. Jordan and E. Wigner, Über das paulische äquivalenzverbot, *Z. Phys.* **47**, 631 (1928).
- [96] L. Funcke, K. Jansen, and S. Kühn, Topological vacuum structure of the Schwinger model with matrix product states, *Phys. Rev. D* **101**, 054507 (2020).
- [97] D. Wecker, M. B. Hastings, and M. Troyer, Progress towards practical quantum variational algorithms, *Phys. Rev. A* **92**, 042303 (2015).
- [98] W. W. Ho and T. H. Hsieh, Efficient variational simulation of non-trivial quantum states, *SciPost Phys.* **6**, 029 (2019).
- [99] R. Wiersema, C. Zhou, Y. de Sereville, J. F. Carrasquilla, Y. B. Kim, and H. Yuen, Exploring entanglement and optimization within the Hamiltonian variational ansatz, *PRX Quantum* **1**, 020319 (2020).
- [100] A. D. McLachlan, A variational solution of the time-dependent Schrodinger equation, *Mol. Phys.* **8**, 39 (1964).
- [101] Y. Suzuki, Y. Kawase, Y. Masumura, Y. Hiraga, M. Nakadai, J. Chen, K. M. Nakanishi, K. Mitarai, R. Imai, S. Tamiya, T. Yamamoto, T. Yan, T. Kawakubo, Y. O. Nakagawa, Y. Ibe, Y. Zhang, H. Yamashita, H. Yoshimura, A. Hayashi, and K. Fujii, Qulacs: A fast and versatile quantum circuit simulator for research purpose, *Quantum* **5**, 559 (2021).
- [102] P. Weinberg and M. Bukov, QuSpin: A Python package for dynamics and exact diagonalisation of quantum many body systems part I: Spin chains, *SciPost Phys.* **2**, 003 (2017).
- [103] G. Pagano, A. Bapat, P. Becker, K. S. Collins, A. De, P. W. Hess, H. B. Kaplan, A. Kyprianidis, W. L. Tan, C. Baldwin, L. T. Brady, A. Deshpande, F. Liu, S. Jordan, A. V. Gorshkov, and C. Monroe, Quantum approximate optimization of the long-range Ising model with a trapped-ion quantum simulator, *Proc. Natl. Acad. Sci. U.S.A.* **117**, 25396 (2020).